

A shell-model study of calcium isotopes towards their drip line

L. Coraggio,¹ G. De Gregorio,^{2,1} A. Gargano,¹ N. Itaco,^{2,1} T. Fukui,³ Y. Z. Ma,⁴ and F. R. Xu⁴

¹*Istituto Nazionale di Fisica Nucleare,*

Complesso Universitario di Monte S. Angelo, Via Cintia, I-80126 Napoli, Italy

²*Dipartimento di Matematica e Fisica, Università degli Studi della Campania “Luigi Vanvitelli”,
viale Abramo Lincoln 5 - I-81100 Caserta, Italy*

³*Yukawa Institute for Theoretical Physics, Kyoto University,
Kitashirakawa Oiwake-Cho, Kyoto 606-8502, Japan*

⁴*School of Physics, and State Key Laboratory of Nuclear Physics and Technology,
Peking University, Beijing 100871, China*

We report in this paper a study in terms of the nuclear shell model about the location of the calcium isotopes drip line. The starting point is considering the realistic two-body potential derived by Entem and Machleidt within chiral perturbation theory at next-to-next-to-next-to-leading order (N^3LO), as well as a chiral three-body force at next-to-next-to-leading order (N^2LO) whose structure and low-energy constants are consistent with the two-body potential. Then we construct the effective single-particle energies and residual interaction needed to diagonalize the shell-model Hamiltonian. The calculated two-neutron separation energies agree nicely with experiment until ^{56}Ca , which is the heaviest isotope whose mass has been measured, and do not show any sign of two-neutron emission until ^{70}Ca . We discuss the role of the choice of the model space in determining the neutron drip line, and also the dependence of the results on the parameters of the shell-model Hamiltonian.

PACS numbers: 21.60.Cs, 21.30.Fe, 21.45.Ff, 27.40.+z

I. INTRODUCTION

The location of the boundaries of the nuclear landscape is an important target in order to understand the limits of the strong force to hold together the nucleons in a bound system.

The search of drip lines is not an easy task from the experimental point of view, due to the extremely low production rates in investigations dealing with the fragmentation of stable nuclei, and the subsequent separation and identification of the products. This is why the possibility of expanding the chart of nuclides is closely linked to the development of facilities providing a new generation of re-accelerated radioactive ion beams as well as of new instrumentation and advanced techniques (see, for example, Ref. [1]). Consequently, theory is in charge to provide further insight on this topic, and also to look for useful tips for experimental studies whose results may help to find evidence of proton/neutron drip lines.

In this context, calcium isotopes are one of the most intriguing subjects to be investigated, since this isotopic chain spans from the neutron-deficient ^{36}Ca , which lies close to the proton drip line, up to ^{60}Ca , that has been recently observed [2] and whose N/Z ratio, equal to 2, classifies it as a very exotic nuclear system. As a matter of fact, the observation of ^{60}Ca draws a line between studies predicting it as a loosely bound nucleus [3–5] and those pushing neutron drip line up to ^{70}Ca [6–9]. Moreover, recent mass measurements of heavy calcium isotopes [10, 11] are helpful to narrow the spread of the theoretical predictions about this yet undiscovered section of the chart of nuclides.

Another interesting aspect is the impulse that the novel experimental results have given to the advance in the-

ory. In Ref. [9] the authors have followed an innovative approach to the study of calcium-isotopes drip line; they have performed a model averaging analysis of the outcome of different density-functional calculations, by way of Bayesian machine learning. The result of their study is that, by considering both experimental information and current density-functional models, ^{68}Ca owns an average posterior probability of about 76% to be bound with respect to the two-neutron emission. It is worth stressing that this study conjugates advances in computational theory - machine-learning methods - with a comparative analysis of energy-density functionals that are constrained to reproduce a variety of nuclear binding energies and radii.

Nuclei approaching the neutron drip line may show exotic features such as an extended neutron distribution and halo. This may be difficult to be reproduced with the harmonic-oscillator basis, since this could provide a slow convergence rate of the calculations. On the above grounds, the authors in Ref. [4] have investigated the evolution of shell structure of neutron-rich calcium isotopes by way of the coupled-cluster method, starting from chiral two- and three-body forces, and including the coupling to the particle continuum in terms of the Berggren basis.

The effects of a neutron skin have been studied in Ref. [12], where the neutron ^{60}Ca S -wave scattering phase shifts have been calculated within the coupled-cluster theory, employing interactions derived from chiral perturbation theory. The authors have found evidence of Efimov physics, namely a discrete scale invariance in three-body systems such as a tight core and two loosely bound nucleons [13].

Neutron-halo features of neutron-rich calcium iso-

topes have been also investigated within the framework of the relativistic-mean-field and complex-momentum-representation method [8], providing indications of a possible halo or giant halo structure of isotopes with $N \geq 40$.

Finally, it is also worth mentioning recent studies about the calcium isotopic chain by way of microscopic many-body approaches - and employing chiral two- and three-body potentials - such as the Bogoliubov many-body perturbation theory [14], the In-Medium Similarity Renormalization Group [15, 16], and the Self-Consistent Green's Function Theory [17].

Our aim is to study heavy calcium isotopes, providing a prediction of their neutron drip line and shell evolution by way of nuclear shell model (SM). The framework is the same of our previous study about the monopole component of the shell-model Hamiltonian for $0f1p$ -shell nuclei, where the single-particle (SP) energies and the two-body matrix elements (TBMEs) of the residual interaction have been derived from two- and three-body forces obtained by way of the chiral perturbation theory (ChPT) [18]. The main difference here is that we consider a larger model space, by including the neutron $0g_{9/2}$ orbital in addition to the $0f1p$ orbitals, a choice that is needed to extend the calculations to isotopes with $N > 40$. We will focus on the relevance of the new SP degree of freedom, and of the induced three-body contributions that appear in the effective SM Hamiltonian H_{eff} to account for many-body correlations in nuclei with more than two valence nucleons [19]. This means that in the derivation of H_{eff} we consider also the interaction of clusters of three-valence nucleons with core excitations as well as with virtual intermediate nucleons scattered above the model space, through density-dependent $H_{\text{eff}}^{\text{S}}$, whose TBMEs change according to the number of valence nucleons.

It should be pointed out that a similar approach has been followed by Holt and coworkers in Refs. [20, 21], where the two-body chiral potential has been renormalized through the $V_{\text{low-}k}$ technique [22] and the effect of many-body correlations in the derivation of H_{eff} has been neglected.

This paper is organized as follows: next section is devoted to present a few details of the derivation of the effective SM Hamiltonian from realistic two- and three-body nuclear potentials, that is framed within the many-body perturbation theory. In Section III the results of the diagonalization of the $H_{\text{eff}}^{\text{S}}$ for the calcium isotopic chain are presented and compared with available data from experiment. We will also show the results obtained previously within a smaller model space [18], those obtained neglecting many-body correlations, and varying the energy of the $0g_{9/2}$ orbital, in order to provide insight on the sensitivity of SM results to the degrees of freedom our $H_{\text{eff}}^{\text{S}}$ account for. Finally, in Section IV we draw the conclusions of present investigation.

II. OUTLINE OF CALCULATIONS

A. The effective shell-model Hamiltonian

The SM parameters, that are needed to diagonalize the SM Hamiltonian, are derived from realistic nucleon-nucleon (NN) and three-body (NNN) potentials, both of them derived within the ChPT at next-to-next-to-next-to-leading order ($N^3\text{LO}$) [23] and at next-to-next-to-leading order ($N^2\text{LO}$), respectively. These potentials consistently share the same nonlocal regulator function, and some low-energy constants (LECs). More precisely, the $N^2\text{LO}$ NNN potential is composed of three components, namely the two-pion (2π) exchange term $V_{3NF}^{(2\pi)}$, the one-pion (1π) exchange plus contact term $V_{3NF}^{(1\pi)}$, and the contact term $V_{3NF}^{(\text{ct})}$. The c_1 , c_3 , and c_4 LECs which characterize these terms are the same as those in the $N^3\text{LO}$ NN potential, and are determined by the renormalization procedure that is employed to fit the NN data [24].

The values of the additional LECs appearing in 1π -exchange and contact terms of the NNN potential, c_D and c_E , have been chosen as $c_D = -1$ and $c_E = -0.34$. They have been determined in no-core shell model calculations [25, 26], by identifying a set of observables in light p -shell nuclei that are strongly sensitive to the c_D value, and then c_E has been constrained to reproduce the binding energies of the $A = 3$ system.

In Appendix of Ref. [27], the details of the calculation of matrix elements of the $N^2\text{LO}$ NNN potential, with a nonlocal regulator, in a harmonic-oscillator (HO) basis can be found.

The Coulomb potential is explicitly taken into account aside the matrix elements of the NN potential. The oscillator parameter $\hbar\omega$ we have employed to compute the matrix elements of the NN and NNN potentials in the HO oscillator basis is equal to 11 MeV, according to the expression $\hbar\omega = 45A^{-1/3} - 25A^{-2/3}$ for $A = 40$ [28].

These nuclear potentials are the foundations to build up the effective SM Hamiltonian H_{eff} that provides SP energies and TBMEs to solve the SM eigenvalue problem. As is well known, H_{eff} accounts for the degrees of freedom that are not explicitly included in the truncated Hilbert space of the configurations that, in our case, is spanned by four $0f1p$ plus $0g_{9/2}$ neutron orbitals outside the doubly-closed ^{40}Ca .

To this end, we need a similarity transformation which arranges, within the full Hilbert space of the configurations, a decoupling of the model space P where the valence nucleons are constrained from its complement $Q = 1 - P$.

We tackle this problem within the time-dependent perturbation theory, namely H_{eff} is expressed through the Kuo-Lee-Ratcliff folded-diagram expansion in terms of the \hat{Q} -box vertex function [29–31].

The \hat{Q} -box is defined in terms of the full nuclear Hamiltonian $H = H_0 + H_1$, where H_0 is the unperturbed com-

ponent and H_1 the interaction one:

$$\hat{Q}(\epsilon) = PH_1P + PH_1Q \frac{1}{\epsilon - QHQ} QH_1P, \quad (1)$$

and ϵ is an energy parameter called ‘‘starting energy’’.

Since the exact calculation of the \hat{Q} -box is impossible, the term $1/(\epsilon - QHQ)$ is expanded as a power series

$$\frac{1}{\epsilon - QHQ} = \sum_{n=0}^{\infty} \frac{1}{\epsilon - QH_0Q} \left(\frac{QH_1Q}{\epsilon - QH_0Q} \right)^n, \quad (2)$$

leading to the perturbative expansion of the \hat{Q} -box. It is useful to employ a diagrammatic representation of this perturbative expansion, which is a collection of Goldstone diagrams that have at least one H_1 -vertex, are irreducible - namely at least one line between two successive vertices does not belong to the model space - and are linked to at least one external valence line (valence linked) [32].

Then, the \hat{Q} -box is employed to solve non-linear matrix equations to derive H_{eff} by way of iterative techniques such as the Kuo-Krenciglowa and Lee-Suzuki ones [33], or graphical non-iterative methods [34]. We have experienced that the latter provide a faster and more stable convergence to the solution of the matrix equation to derive H_{eff} , and are the ones we have employed in present work.

We include in our \hat{Q} -box expansion one- and two-body Goldstone diagrams through third order in the NN potential and up to first order in the NNN one. A complete list of diagrams with NN vertices can be found in Ref. [31], while the diagrams at first order in NNN potential, as well as their analytical expressions, are reported in Refs. [18, 27]. It is worth pointing out that these expressions are the coefficients of the one-body and two-body terms arising from the normal-ordering decomposition of the three-body component of a many-body Hamiltonian [35]. In Ref. [21], Holt and coworkers, using a similar approach to study Ca isotopes, have shown that the uncertainty linked to neglecting contributions beyond the normal-ordered two-body components (residual NNN forces) is small.

Since we are going to study many-valence nucleon systems, we should derive many-body H_{eff} s which depend on the number of valence particles. This means that the \hat{Q} -box should include at least contributions from three-body diagrams accounting for the interaction via the two-body force of the valence nucleons with configurations outside the model space.

Since we employ SM codes which cannot perform the diagonalization of a three-body H_{eff} [36, 37], we derive a density-dependent two-body term from the three-body contribution arising at second order in perturbation theory. Namely, nine one-loop diagrams (see the graph (b) in Fig. 1) are calculated from the corresponding diagrams reported in Fig. 3 of Ref. [19].

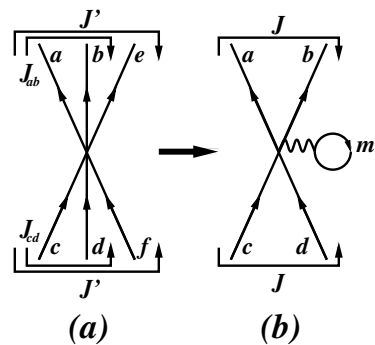


FIG. 1. Density-dependent two-body contribution that is obtained from a three-body one. Graph (b) is obtained by summing over one incoming and outgoing particle of the three-body graph (a).

Their explicit form is reported in Ref. [18], and depends on the unperturbed occupation density ρ_m of the orbital j_m , leading to the derivation of H_{eff} s depending on the number of valence protons and neutrons. The density-dependent H_{eff} s differ only in their TBMEs since, as can be seen in Fig. 1, these one-loop diagrams are two-body terms.

It should be recalled that, since the neutron $0g_{9/2}$ orbital may couple with the $0f_{7/2}$ one to the total angular momentum $J^\pi = 1^-$, the results of the diagonalization of the shell-model Hamiltonian within the model space with 5 neutron orbitals might be affected somehow by the spurious center-of-mass motion [38].

In order to check if these spuriousities are under control, we have also performed calculations to separate in energy the excitations originated by the internal degrees of freedom from those with spurious center-of-mass components by following the procedure suggested by Gloeckner and Lawson [39].

According to Ref. [39], the modified shell-model Hamiltonian H' should be diagonalized:

$$H' = H_{\text{eff}} + H_\beta, \quad (3)$$

where H_β is β times the center-of-mass excitation energy of the A -nucleon system

$$H_\beta = \beta \left\{ \frac{(\sum_{i=1}^A \mathbf{p}_i)^2}{2Am} + \frac{m\omega^2}{2A} \left(\sum_{i=1}^A \mathbf{r}_i \right)^2 - \frac{3}{2} \hbar\omega \right\}. \quad (4)$$

The spurious components are then pushed up in energy by increasing the parameter β , so that one can assume that the low-energy spectrum is weakly influenced by the above components. We have performed calculations using values of β such that $\gamma = \beta \frac{\hbar\omega}{A}$ is equal to 10 MeV and 15 MeV in order to evaluate the role of the center-of-mass spuriousities [40], and the results will be reported in Section III.

B. Convergence properties of H_{eff}

We now discuss the convergence properties of our H_{eff} s, an issue that needs to be examined since the input chiral NN and NNN potentials have not been modified by way of any renormalization procedure.

In Ref. [18] we have extensively discussed the order-by-order behavior of the perturbative expansion of the \hat{Q} -box, as well as the convergence with respect to the dimension of the space of the intermediate states, considering the systems with one- and two-valence neutrons, namely ^{41}Ca and ^{42}Ca , respectively. We recall that we express the number of intermediate states as a function of the maximum allowed excitation energy of the intermediate states expressed in terms of the oscillator quanta N_{max} [31], and include intermediate states with an unperturbed excitation energy up to $E_{\text{max}} = N_{\text{max}}\hbar\omega$. Because of our present limitation of the storage of the total number of TBMEs, we can include, for ^{40}Ca core, a maximum number of intermediate states that do not exceed $N_{\text{max}}=18$.

In Ref. [18], we have shown that this value is not large enough to provide convergence of the SP spectrum of ^{41}Ca , since the chosen HO parameter is 11 MeV and the cutoff of both NN and NNN potentials is slightly larger than 2.5 fm^{-1} , this values leading to a value of N_{max} to be at least 26. However, this does not affect the convergence of the energy spacings that are stable with respect to the increase in the number of intermediate states from $N_{\text{max}} \approx 12 - 14$ on for both ^{41}Ca and ^{42}Ca , as already shown in Ref. [18].

In this work we will show the convergence properties of H_{eff} by considering a more complex system, such as ^{50}Ca , which is characterized by 10 valence neutrons. By studying this system, we can test the perturbative behavior of H_{eff} s that include density-dependent contributions which account for three-body correlations. It is worth pointing out that our choice is challenging, since ^{50}Ca exhibits a structure that is more collective than other neighbor isotopes, whose closure properties provide a simpler structure of the wave functions.

In Fig. 2 we report the low-lying states of ^{50}Ca spectrum, which have been obtained employing H_{eff} s starting from \hat{Q} -boxes at first-, second-, and third-order in perturbation theory, and their Padé approximant [2|1] [41], while the number of intermediate states is the largest we can manage, i.e. $N_{\text{max}}=18$.

We employ the Padé approximant in order to obtain a better estimate of the convergence value of the perturbation series [31], as suggested in Ref. [42].

The results show a very satisfactory perturbative behavior of H_{eff} with respect to the order-by-order convergence.

We consider now the dependence of H_{eff} as a function of the number of intermediate states included in the calculation of the \hat{Q} -box second- and third-order diagrams.

As it as been mentioned before, $N_{\text{max}}=18$ does not provide a convergent SP spectrum of ^{41}Ca , but in Ref.

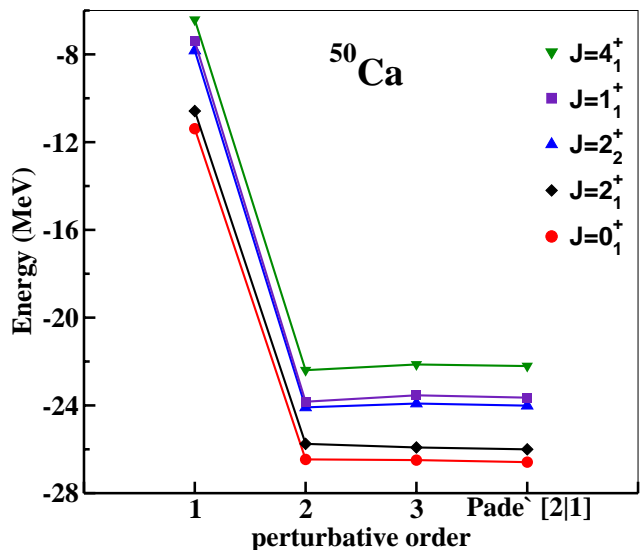


FIG. 2. Low-lying energy spectrum of ^{50}Ca , obtained starting from \hat{Q} -boxes at first-, second-, and third-order in perturbation theory, and their Padé approximant [2|1].

[18] we have shown that the SP spacings are stable. Consequently, from now on for our calculations we consider SP spacings obtained from the theory but the value of the SP energy of the neutron $0f_{7/2}$ orbital is fixed at -8.4 MeV , consistently with the experimental value in ^{41}Ca [43].

In Fig. 3 they are reported the energy spectra of ^{50}Ca , obtained diagonalizing the density-dependent H_{eff} calculated employing the Padé approximant [2|1] of the \hat{Q} -box, and including a number of intermediates states ranging from $N_{\text{max}}=2$ to 18. Theoretical results are also compared with experiment [44].

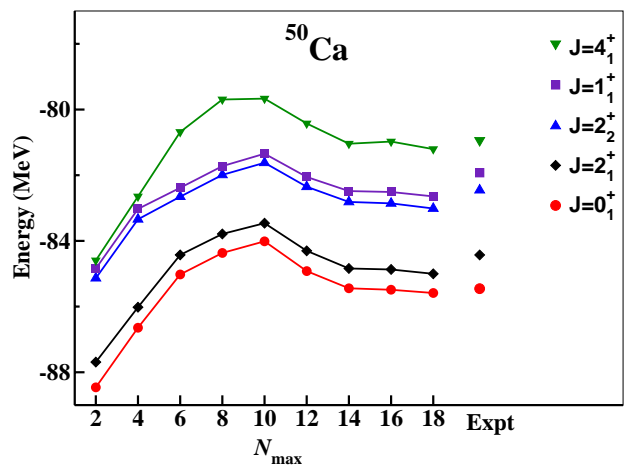


FIG. 3. Low-lying energy spectrum of ^{50}Ca as a function of the number of intermediate states included in the perturbative calculation of the \hat{Q} -box.

TABLE I. Theoretical proton (ϵ_π) and neutron (ϵ_ν) SP energies (in MeV), referred to the $0f_{7/2}$ orbital.

	ϵ_π	ϵ_ν
$0f_{7/2}$	0.0	0.0
$0f_{5/2}$	6.3	8.2
$1p_{3/2}$	2.5	3.2
$1p_{1/2}$	4.4	5.3
$0g_{9/2}$		9.9

This is a test for our theoretical SP spacings and, especially, TBMEs, and we observe that ^{50}Ca spectrum converges from $N_{\text{max}}=14$ on. This leads to the conclusion that the SP spacings and TBMEs of our H_{eff} , calculated with $N_{\text{max}}=18$, can be considered substantially stable. It is worth pointing out that in Ref. [18] the same study has been performed for two-valence neutron system ^{42}Ca , and in that case the convergence rate is much faster.

We conclude this section by reporting in Table I the proton and neutron SP energies $\epsilon_\pi, \epsilon_\nu$, calculated with respect to $0f_{7/2}$. The proton-proton and proton-neutron H_{eff} channel has been derived by considering a proton model space composed by the four orbitals belonging to the $0f1p$ shell. In the Supplemental Material [45] the TBMEs of H_{eff} s for systems with 2 and 10 valence nucleons can be found.

III. RESULTS

In our previous study about nuclei belonging to $0f1p$ shell, we have evidenced the crucial role played by the NNN component of nuclear Hamiltonians derived by way of ChPT, in order to provide SP energies and TBMEs that may reproduce the shell evolution as observed from the experiment [18]. We have seen that SP energies and TBMEs of H_{eff} derived only from the NN component own deficient monopole components, which cannot provide the shell closures at $N = 28$ for both ^{48}Ca and ^{56}Ni .

On the above grounds, in our present work we are going to deal only with H_{eff} s that are derived with NN and NNN components.

We start showing in Table II our calculated two-neutron separation energies up to ^{70}Ca , compared with the available experimental data [10, 11, 43]. As previously mentioned, the neutron SP energies reported in Table I are shifted to reproduce the experimental g.s. energy of ^{41}Ca with respect to ^{40}Ca .

The results of our calculations, performed by way of the shell-model code KSHELL [37], are also presented in Fig. 4 (black diamonds, continuous line) to compare them with those we have obtained in Ref. [18] where the model space we have employed does not include the $0g_{9/2}$ orbital (blue triangles). We report the experimental values as red dots and, as mentioned in Section II, also the

results obtained diagonalizing the Hamiltonian H' in Eq. 3 with values of $\gamma = 10$ MeV (dashed black line) and 15 MeV (dash-dotted black line).

We note that closure properties, related to the filling of SP orbitals, are reflected in the behavior of both experimental and theoretical S_{2n} .

As can be seen, data and calculated values show a rather flat behavior up to $N = 28$, then a sudden drop occurs at $N = 30$ that is a signature of the shell closure due to the $0f_{7/2}$ filling. Another decrease appears at $N = 34$ because at that point the valence neutrons start to occupy the $1p_{1/2}$ and $0f_{5/2}$ orbitals. Then, from $N = 36$ on, the calculated curve is rather flat matching the filling of $0f_{5/2}, 0g_{9/2}$ orbitals.

The results obtained with both model spaces, the one considered in present work with five neutron orbitals and the other with four orbitals from Ref. [18], follow closely the behavior of the experimental S_{2n} up to $N = 34$, while those obtained in our previous work provide an energy drop between $N = 34$ and 36 much stronger than the observed one.

It should be also pointed out that the results obtained with the Hamiltonian H' for values of the parameter $\gamma = 10, 15$ MeV evidence that the spuriousities introduced by the center-of-mass motion are under control for the calculation of two-neutron separation energies.

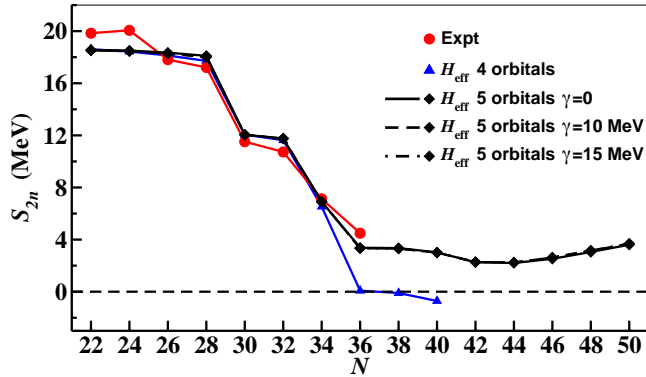
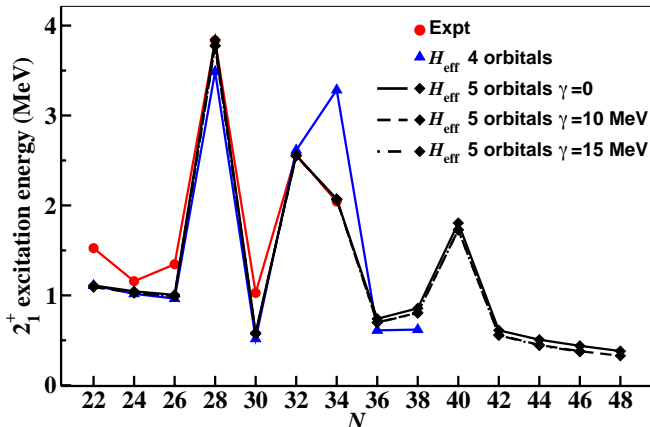
This shell-closure properties of calcium isotopes can obviously be also observed in the evolution of the excitation energies of the yrast $J^\pi = 2^+$ states with respect to the number of neutrons N , as reported in Fig. 5.

It is noteworthy to observe that we obtain a better agreement with experiment by including the $0g_{9/2}$ orbital. In fact, within such a model space, we better reproduce the subshell closure at $N = 34$ and predict bound calcium isotopes at least up to $N = 50$. Actually, the results obtained without $0g_{9/2}$ orbital provide, in contrast with data, a raise of the excitation energy of the $J^\pi = 2^+_{1/2}$ state between $N = 32$ and 34, and predict the calcium drip line located at $N = 38$ at variance with the recent observation of a bound ^{60}Ca [2].

This testifies the need of a model space larger than the standard one spanned by the $0f1p$ orbitals to perform a reliable investigation of heaviest calcium isotopes.

TABLE II. Calculated and experimental two-neutron separation energies (in MeV). Data are taken from Refs. [10, 11, 43].

	^{42}Ca	^{44}Ca	^{46}Ca	^{48}Ca	^{50}Ca	^{52}Ca	^{54}Ca	^{56}Ca	^{58}Ca	^{60}Ca	^{62}Ca	^{64}Ca	^{66}Ca	^{68}Ca	^{70}Ca
Calculated S_{2n}	18.562	18.514	18.351	18.105	12.054	11.754	6.914	3.377	3.347	3.017	2.266	2.202	2.526	3.048	3.605
Experimental S_{2n}	19.844	20.064	17.810	17.218	11.517	10.73	7.127	4.492							

FIG. 4. Experimental and theoretical two-neutron separation energies for calcium isotopes from $N = 22$ to 50. Data are taken from [10, 11, 43]. See text for details.FIG. 5. Experimental and theoretical excitation energies of the yrast $J^\pi = 2^+$ states for calcium isotopes from $N = 22$ to 50. See text for details.

In Fig. 5 we have also reported the results we obtain by employing the Hamiltonian H' in Eq. 3 with values of $\gamma = 10$ MeV (dashed black line) and 15 MeV (dash-dotted black line). As can be seen, the center-of-mass spuriousities provide a little contribution also for the calculation of the excitation energies of the yrast $J^\pi = 2^+$.

It is now worth recalling that in the Introduction we mentioned about the role that continuum states may play in isotopic chains approaching their drip lines. In a recent paper we investigated the neutron drip line of oxygen isotopes [46], which is experimentally placed at $N = 24$, by writing the many-body Hamiltonian in the Berggren ba-

sis and deriving a H_{eff} , built up in terms of the present chiral NN and NNN potentials, that accounts for continuum states. We have observed that this adds an additional repulsive effect to the one provided by the NNN component of the nuclear potential, and leads to a better agreement with experiment too.

A similar procedure might be employed also to study calcium isotopes, but the present limits of our computational resources prevent to derive H_{eff} with the same accuracy we have done within the HO basis, and we are working to implement continuum effects in the future also for fp isotopic chains.

There are two points that should be worth discussing in connection with the outcome of our calculations, namely the effects of many-body correlations and the sensitivity of our results with respect to the position of the neutron $0g_{9/2}$ orbital.

As regards the first one, we have already mentioned in the previous section that we include the effect of second-order three-body diagrams, which, for systems with more than 2 valence nucleons, account for the interaction of the valence nucleons with core excitations as well as with virtual intermediate nucleons scattered above the model space, via the NN potential [47].

This, as reported in Section II, has been done by deriving a density-dependent two-body contribution at one-loop order from the three-body correlation diagrams, and summing over the partially-filled model-space orbitals, to overcome the limitations of our SM codes. Here, we want to show the difference of the results of SM calculations performed including or not the effects of such three-body correlations.

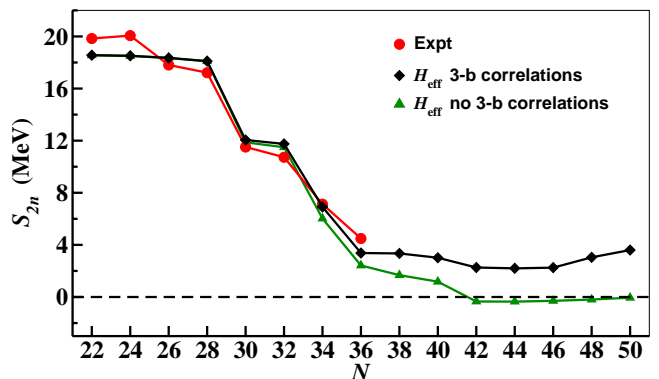


FIG. 6. Same as in Fig. 4, but including the results obtained without three-body correlations (green triangles).

To this end, in Figs. 6,7 we compare experimental two-

neutron separation energies and excitation energies of yrast $J^\pi = 2^+$ states (red dots), respectively, of calcium isotopes up to $N = 50$, with the results of SM calculations obtained including the effect of three-body correlations (black diamonds), which means considering density-dependent H_{eff} s, and with those obtained with H_{eff} derived for just the two-valence nucleon system (green triangles).

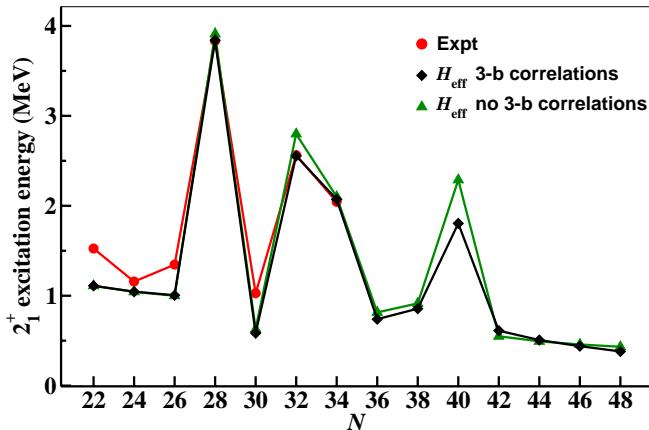


FIG. 7. Same as in Fig. 5, but including the results obtained without three-body correlations (green triangles).

As can be seen, the effect of three-body correlations increases with the number of valence nucleons, and starts to be substantial from $N = 34$ on. The role of this effect is far more important for the ground-state energies than the calculated excitation energies, and it is extremely relevant to soundly determine the drip line. In fact, without considering many-body correlations we see that the drip line of calcium isotopes is located at $N = 40$, while the attractive contribution of second-order correlation diagrams shifts the last bound nucleus at least to ^{70}Ca .

The second point that should be examined is the correlation between the SP spacings we have employed for our calculations, as reported in Table I, and the evolution of the calculated two-neutron separation energies. Our SP spacings have been derived as the energy spectrum of the effective Hamiltonian of one-valence nucleon systems, and they should reproduce the experimental spectra of SP states in ^{41}Ca (and ^{41}Sc for protons).

As a matter of fact, the experimental information about the spectroscopic factors of ^{41}Ca are rather scanty, and in fact the observed counterpart of the second column in Table I is missing. However, there are three well-identified SP states in ^{49}Ca , whose spectroscopic factors with respect to doubly-closed ^{48}Ca have been measured [44, 48], and they are reported together with the calculated values in Table III.

TABLE III. Experimental negative-parity energy levels (in MeV) of ^{49}Ca [44] $J^\pi = \frac{3}{2}^-, \frac{1}{2}^-, \frac{5}{2}^-$ states, compared with the calculated ones. The values in parenthesis are the one-neutron pickup spectroscopic factors [48].

J^π	Expt.	Calc.
$\frac{3}{2}^-$	0.000 (0.84)	0.000 (0.96)
$\frac{1}{2}^-$	2.023 (0.91)	1.824 (0.97)
$\frac{5}{2}^-$	3.585 (0.11)	3.710 (0.0001)
$\frac{7}{2}^-$	3.991 (0.84)	4.191 (0.96)

The comparison between data and theory in Table III, as well as the correct reproduction of the excitation energy of yrast $J^\pi = 2^+$ state in ^{48}Ca - which is strongly linked to the SP energy spacing $\epsilon_{1p_{3/2}} - \epsilon_{0f_{7/2}}$ -, indicate that the calculated SP spacings of natural-parity $0f1p$ orbitals are reliable. As regards the position of the neutron $0g_{9/2}$ orbital, there is no clear experimental indication if our calculated value is reasonable or not.

We have then calculated the odd-even mass difference around ^{68}Ni that, because of the observed shell closure of nickel isotopes at $N = 40$, has a strong dependence on the energy gap between the $0g_{9/2}$ and $0f_{5/2}$ orbitals, and whose experimental value is 3.2 MeV [43]. The calculation cannot be performed exactly with our present computational resources [37, 49], so we truncate the dimension of the eigenvalue problem by decomposing the eigenfunctions in terms of broken pairs, and retaining only the components with generalized seniority $v_g \leq 4$, the results changing about 0.5% between $v_g = 3$ and 4. It turns out that our value is 4.2 MeV, 1 MeV larger than the observed one, and indicating that the SP spacing $\epsilon_{0g_{9/2}} - \epsilon_{0f_{5/2}}$ could be overestimated by the same amount.

On the above grounds, we have investigated the sensitivity of our results to the position of the $0g_{9/2}$ SP state, by raising and lowering its energy by 1 MeV with respect to the calculated value.

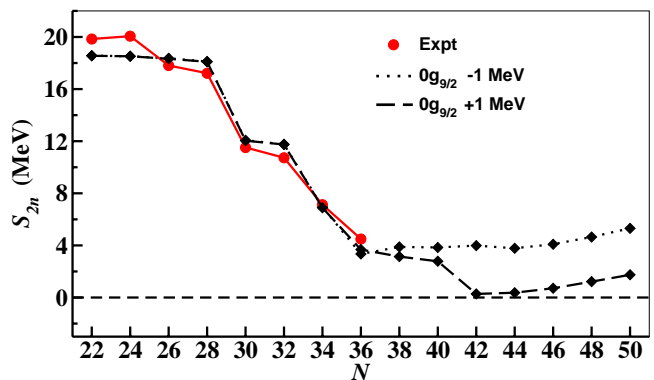


FIG. 8. Same as in Fig. 4, but with calculated values are obtained raising (dashed line) and lowering (dotted line) $\epsilon_{0g_{9/2}}$ by 1 MeV.

In Figs. 8 and 9 we report the results obtained with these two new values of $\epsilon_{0g_{9/2}}$ for both the two-neutron separation energies and the excitation energies of yrast $J^\pi = 2^+$, respectively.

We observe that up to $N = 40$ the results barely differ each other as well as from those with the set of SP energies in Table I, and consequently the available experimental values cannot discriminate about the choice of $0g_{9/2}$ SP energy. From $N = 40$ a clear distinction is observed: raising $\epsilon_{0g_{9/2}}$ by 1 MeV we obtain that ^{62}Ca is loosely bound with respect to ^{60}Ca , and a strong shell closure appears at $N = 40$. This shell closure disappears lowering $\epsilon_{0g_{9/2}}$ by 1 MeV, leading to the conclusion that a future measurement of the experimental excitation energy of the yrast $J^\pi = 2^+$ state may provide insight on the location of calcium isotopes drip line.

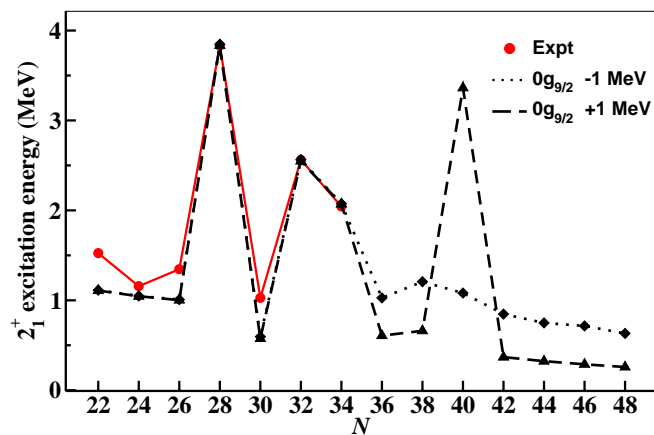


FIG. 9. Same as in Fig. 5, but with calculated values are obtained raising (dashed line) and lowering (dotted line) $\epsilon_{0g_{9/2}}$ by 1 MeV.

IV. CONCLUSIONS

This study is focussed on the location of the neutron drip line of calcium isotopes, as predicted by nuclear shell-model calculations.

It is grounded on the results we have obtained in Ref. [18], where, starting from two- and three-nucleon potentials derived within the chiral perturbation theory, we have calculated effective SM Hamiltonians able to reproduce the observed closure properties of calcium isotopes and other $0f1p$ isotopic chains. Here, in order to improve the depiction of heavier systems, the model space has been enlarged by adding the neutron $0g_{9/2}$ orbital.

Choosing a larger model space, we have improved the description of the few observables in $^{54,56}\text{Ca}$ with respect to the results obtained without $0g_{9/2}$ orbital, and have also been able to describe ^{60}Ca as a bound system, consistently with a recent experiment [2].

The main outcome of our investigation is, however,

the fact that according to our results the calcium isotopic chain is bound up to ^{70}Ca , at least, a result that is consistent with the recent Bayesian analysis of different density-functional calculations developed by Neufcourt and coworkers [9]. We have therefore also studied the relationship between our theoretical tools and our prediction of the limits of calcium isotopes as bound systems.

More precisely:

- a) we have studied the role played by the inclusion of three-body correlations to calculate binding energies. As a matter of fact, calcium drip line would be placed at $N = 40$ by neglecting these attractive contributions.
- b) Since the position of the $0g_{9/2}$ single-particle energy is quite relevant when the filling of this orbital starts from $N = 40$ on, we have investigated the sensitivity of both the two-neutron separation energies and the behavior of yrast $J^\pi = 2^+$ excitation energy to this shell-model parameter. At present, available data do not allow to verify the reliability of our calculated prediction of $0g_{9/2}$ SP energy, at variance with the $0f1p$ orbitals, and we have found that the location of calcium drip line may be correlated with this quantity. In particular, our calculations indicate that the measurement of the yrast $J^\pi = 2^+$ excitation energy in ^{60}Ca could be pivotal to rule out predictions about the last bound calcium isotope.

We consider this last point quite intriguing, since experimental investigations of isotopes heavier than ^{60}Ca may be very challenging in a near future, and theory is in charge to point to spectroscopic properties that at the same time should be easier to be measured and provide informations about the “terra incognita” of exotic nuclear systems.

ACKNOWLEDGEMENTS

This work has been supported by the National Key R&D Program of China under Grant No. 2018YFA0404401, the National Natural Science Foundation of China under Grants No. 11835001 and No. 11921006, and the CUSTIPEN (China-US Theory Institute for Physics with Exotic Nuclei) funded by the US Department of Energy, Office of science under Grant No. DE-SC0009971. We acknowledge the CINECA award under the ISCR initiative through the INFN-CINECA agreement, for the availability of high performance computing resources and support, and the High-performance Computing Platform of Peking University for providing computational resources. G. De Gregorio acknowledges the support by the funding program “VALERE” of Università degli Studi della Campania “Luigi Vanvitelli”.

-
- [1] M. Thoennessen, Rep. Prog. Phys. **76**, 056301 (2013).
- [2] O. B. Tarasov, D. S. Ahn, D. Bazin, N. Fukuda, A. Gade, M. Hausmann, N. Inabe, S. Ishikawa, N. Iwasa, K. Kawata, et al., Phys. Rev. Lett. **121**, 022501 (2018).
- [3] J. Meng, H. Toki, J. Y. Zeng, S. Q. Zhang, and S.-G. Zhou, Phys. Rev. C **65**, 041302 (2002).
- [4] G. Hagen, M. Hjorth-Jensen, G. R. Jansen, R. Machleidt, and T. Papenbrock, Phys. Rev. Lett. **109**, 032502 (2012).
- [5] H. Hergert, S. K. Bogner, T. D. Morris, S. Binder, A. Calci, J. Langhammer, and R. Roth, Phys. Rev. C **90**, 041302 (2014).
- [6] M. Bhattacharya and G. Gangopadhyay, Phys. Rev. C **72**, 044318 (2005).
- [7] W.-C. Chen and J. Piekarewicz, Physics Letters B **748**, 284 (2015).
- [8] X.-N. Cao, Q. Liu, Z.-M. Niu, and J.-Y. Guo, Phys. Rev. C **99**, 024314 (2019).
- [9] L. Neufcourt, Y. Cao, W. Nazarewicz, E. Olsen, and F. Viens, Phys. Rev. Lett. **122**, 062502 (2019).
- [10] F. Wienholtz, D. Beck, K. Blaum, C. Borgmann, M. Breitenfeldt, R. B. Cakirli, S. George, F. Herfurth, J. Holt, M. Kowalska, et al., Nature (London) **498**, 346 (2013).
- [11] S. Michimasa, M. Kobayashi, Y. Kiyokawa, S. Ota, D. S. Ahn, H. Baba, G. P. A. Berg, M. Dozono, N. Fukuda, T. Furuno, et al., Phys. Rev. Lett. **121**, 022506 (2018).
- [12] G. Hagen, P. Hagen, H.-W. Hammer, and L. Platter, Phys. Rev. Lett. **111**, 132501 (2013).
- [13] V. Efimov, Physics Letters B **33**, 563 (1970).
- [14] A. Tichai, P. Arthuis, T. Duguet, H. Hergert, V. Somà, and R. Roth, Physics Letters B **786**, 195 (2018).
- [15] J. Simonis, S. R. Stroberg, K. Hebeler, J. D. Holt, and A. Schwenk, Phys. Rev. C **96**, 014303 (2017).
- [16] J. Hoppe, C. Drischler, K. Hebeler, A. Schwenk, and J. Simonis, Phys. Rev. C **100**, 024318 (2019).
- [17] V. Somà, P. Navrátil, F. Raimondi, C. Barbieri, and T. Duguet, Phys. Rev. C **101**, 014318 (2020).
- [18] Y. Z. Ma, L. Coraggio, L. De Angelis, T. Fukui, A. Gargano, N. Itaco, and F. R. Xu, Phys. Rev. C **100**, 034324 (2019).
- [19] A. Polls, H. Mütter, A. Faessler, T. T. S. Kuo, and E. Osnes, Nucl. Phys. A **401**, 124 (1983).
- [20] J. D. Holt, T. Otsuka, A. Schwenk, and T. Suzuki, J. Phys. G **39**, 085111 (2012).
- [21] J. D. Holt, J. Menéndez, J. Simonis, and A. Schwenk, Phys. Rev. C **90**, 024312 (2014).
- [22] S. Bogner, T. T. S. Kuo, L. Coraggio, A. Covello, and N. Itaco, Phys. Rev. C **65**, 051301(R) (2002).
- [23] D. R. Entem and R. Machleidt, Phys. Rev. C **66**, 014002 (2002).
- [24] R. Machleidt and D. R. Entem, Phys. Rep. **503**, 1 (2011).
- [25] P. Navrátil, V. G. Gueorguiev, J. P. Vary, W. E. Ormand, and A. Nogga, Phys. Rev. Lett. **99**, 042501 (2007).
- [26] P. Maris, J. P. Vary, and P. Navrátil, Phys. Rev. C **87**, 014327 (2013).
- [27] T. Fukui, L. De Angelis, Y. Z. Ma, L. Coraggio, A. Gargano, N. Itaco, and F. R. Xu, Phys. Rev. C **98**, 044305 (2018).
- [28] J. Blomqvist and A. Molinari, Nucl. Phys. A **106**, 545 (1968).
- [29] T. T. S. Kuo and E. Osnes, *Lecture Notes in Physics*, vol. 364 (Springer-Verlag, Berlin, 1990).
- [30] M. Hjorth-Jensen, T. T. S. Kuo, and E. Osnes, Phys. Rep. **261**, 125 (1995).
- [31] L. Coraggio, A. Covello, A. Gargano, N. Itaco, and T. T. S. Kuo, Ann. Phys. (NY) **327**, 2125 (2012).
- [32] T. T. S. Kuo, S. Y. Lee, and K. F. Ratcliff, Nucl. Phys. A **176**, 65 (1971).
- [33] K. Suzuki and S. Y. Lee, Prog. Theor. Phys. **64**, 2091 (1980).
- [34] K. Suzuki, R. Okamoto, H. Kumagai, and S. Fujii, Phys. Rev. C **83**, 024304 (2011).
- [35] M. Hjorth-Jensen, M. P. Lombardo, and U. van Kolck, eds., *Lecture Notes in Physics*, vol. 936 (Springer, Berlin, 2017).
- [36] E. Caurier, G. Martínez-Pinedo, F. Nowacki, A. Poves, and A. P. Zuker, Rev. Mod. Phys. **77**, 427 (2005).
- [37] N. Shimizu, T. Mizusaki, Y. Utsuno, and Y. Tsunoda, Computer Physics Communications **244**, 372 (2019).
- [38] J. P. Elliott and T. H. R. Skyrme, Proc. R. Soc. Lond. A **232**, 561 (1955).
- [39] D. H. Gloeckner and R. D. Lawson, Phys. Lett. B **53**, 313 (1974).
- [40] L. Liu, T. Otsuka, N. Shimizu, Y. Utsuno, and R. Roth, Phys. Rev. C **86**, 014302 (2012).
- [41] G. A. Baker and J. L. Gammel, *The Padé Approximant in Theoretical Physics*, vol. 71 of *Mathematics in Science and Engineering* (Academic Press, New York, 1970).
- [42] H. M. Hoffmann, Y. Starkand, and M. W. Kirson, Nucl. Phys. A **266**, 138 (1976).
- [43] G. Audi, A. H. Wapstra, and C. Thibault, Nucl. Phys. A **729**, 337 (2003).
- [44] Data extracted using the NNDC On-line Data Service from the ENSDF database, file revised as of March 15, 2019., URL <https://www.nndc.bnl.gov/ensdf>.
- [45] See Supplemental Material at [URL will be inserted by publisher] for the list of two-body matrix elements of the shell-model Hamiltonian H_{eff} , derived for 2- and 10-valence nucleon systems.
- [46] Y. Ma, F. Xu, L. Coraggio, B. Hu, J. Li, T. Fukui, L. D. Angelis, N. Itaco, and A. Gargano, Physics Letters B **802**, 135257 (2020).
- [47] P. J. Ellis and E. Osnes, Rev. Mod. Phys. **49**, 777 (1977).
- [48] Y. Uozumi, O. Iwamoto, S. Widodo, A. Nohtomi, T. Sakae, M. Matoba, M. Nakano, T. Maki, and N. Koori, Nucl. Phys. A **576**, 123 (1994).
- [49] E. Caurier and G. Martínez-Pinedo, Nucl. Phys. A **704**, 60 (2002).